Asian Journal of Chemistry; Vol. 27, No. 2 (2015), 597-603

ASIAN JOURNAL OF CHEMISTRY

http://dx.doi.org/10.14233/ajchem.2015.17072

Synthesis, Characterization and Calculated Studies of L-Tryptophan Condensation 1,3-Benzenedialdehyde Schiff Base Co(II) and Mn(II) Complexes

X.D. LI[1,*], M.M. AN[2], C.L. LIU[3], C.Q. WANG[1] and X.F. WANG[1]

[1]College of Life Science and Chemistry, Tianshui Normal University, Tianshui 741001, Gansu provice, P.R. China
[2]College of literature and history, Tianshui Normal University, Tianshui 741001, Gansu Province, P.R. China
[3]Faculty of Chemical Engineering, Kunming University of Science and Technology, Kunming, Yunnan 650224, P.R. China

*Corresponding author: Tel: +86 938 8367717; E-mail: lixxxd@163.com

Received: 18 January 2014; *Accepted*: 5 May 2014; *Published online*: 10 January 2015; AJC-16627

New Schiff base ligand H_2L and corresponded to Co(II) and Mn(II) transition metal complexes were prepared with L-tryptophan and 1,3-benzenedialdehyde by condensation reaction. Their structures were characterized by means of elemental analysis, IR, ^1H NMR and thermal analyses. The structural and electronic properties of the studied molecules were investigated theoretically by performing density functional theory (DFT) and natural bond orbital theory (NBO) at the B3LYP method and 6-311+G(d, p) level to access reliable results to the experimental values. The results show that the $CoL{\cdot}H_2O$ and $MnL{\cdot}H_2O$ complexes contain one crystal water molecule, the four oxygen atoms of ligand H_2L coordinated with Co(II) ions were located at the four vertices of the tetrahedron. The HOMO-LUMO energy gap showed that the indole ring to the unoccupied orbitals of Co(II) with an energy gap of 0.125 a.u, it imply that the $CoL{\cdot}H_2O$ complex has higher catalytic activity and selectivity than $MnL{\cdot}H_2O$.

Keywords: Schiff base metal complexes, Tetrahedral coordination, DFT theoretical investigation, HOMO-LUMO energy gap.

INTRODUCTION

Schiff bases are compounds containing an azomethine group (-C=N-), have been attention for many years ago[1-4]. The remarkable electronic and striking tenability of Schiff bases make them to be among the most widely used organic compounds[5-8]. The special π-system in a Schiff base often imposes a geometrical constriction and affects the electronic structure as well. Their metal complexes are applied in many different areas such as catalysts, polymer stabilizers, pigments and dyes and so on[9-14]. Comparing with metalloporphyrins, Schiff base complexes exhibited the structure is relatively simple, the process of synthesis is more easily and the advantages of prominent catalytic activity and products selectivity[9]. Nowadays, it becomes a new class full of development prospect of the catalytic system. The early research results have been confirmed that the Schiff base metals complexes can activate molecular oxygen in oxidation reaction and with molecular oxygen as oxygen source catalytic oxidation with multiple activity a-H atoms have a C=C double bond of the active compounds[14,15]. Especially, during the process of oxidation cyclohexene with molecular oxygen, the conversion and selectivity for 2-cyclohexen-1-ol and 2-cyclohexen-1-one are also improved for the highest catalytic activity of Schiff base metal complexes[14,16,17]. Therefore, base on our previous research results in oxidation cyclohexene of Schiff base metal complexes, a new Schiff base $CoL{\cdot}H_2O$ and $MnL{\cdot}H_2O$ complexes were synthesized successfully by using L-tryptophan and 1,3-Benzenedialdehyde (Fig. 2.). This kind of structure complexes is similar to Jacobsen *et al.*[18] and Katsuki *et al.*[19] type synthetic Salen schiff base complexes structure characteristics. But synthetic process is simple compared with synthesis chiral Schiff base complexes and the Schiff base ligands with containing four oxygen ions donor atoms in their structures, act as good chelating agents for the Co(II) and Mn(II) transition metal ions. Comparing with the traditional Schiff base with N atoms coordinating transition metal, the ligand has strong coordination ability. At the same time, the geometries, the atomic net charge distribution and the main component of front orbital of corresponding to Schiff base ligands and complexes were studied by using the density functional theory (DFT) of Gaussian 09W procedure and electrophilic reaction functional of Fukui wavefunction analyzer software methods.

EXPERIMENTAL

L-Tryptophan, 1,3-benzenedialdehyde and the organic solvents were of reagent grade and it was offered to chemical supplier and solvents were dried and distilled by standard methods before using.

Elemental analyses for carbon, hydrogen and nitrogen were carried out on a Varia EL-III CHN elemental analyzer. The infrared spectrum was recorded on an Brucker EQUIOX-55. IR spectrometer in the 4000-400 cm^{-1} region with KBr pellets. The ^{1}HNMR spectra were recorded in DMSO-d_6 on Bruker Arance II400M analyzers, where the chemical shifts were determined relative to the solvent peaks. The thermal analyses (TG, DTG and DTA) were carried out in dynamic atmosphere (15 mL min^{-1}) with a heating rate of 10 °C min^{-1} using pyris diamond TG-DTA thermal analyzers.

Synthesis of H_2L Schiff base: A solution of L-tryptophan (2.042 g, 10 mmol) and NaOH (6 g, 150 mmol) in 50 mL ethanol was stirred for 0.5 h and then 20 mL ethanol solution of 1,3-benzenedialdehyde (0.67 g, 5 mmol) was added dropwise at room temperature for 0.5 h. After the reaction solution was continuously stirred at 60 °C for 6 h, abundant of white solid product was appeared, followed by cooling for filtration. The product obtained was filtered off, washed with ethanol then dried *in vacuo* (60 °), to give Schiff base ligand H_2L as a white solid is only soluble in dimethyl sulfoxide (DMSO) and N,N-dimethylformamide (DMF). Yield: 1.16 g (86 %). Elemental analysis for $C_{30}H_{26}N_4O_4$: Calcd. (%): C, 71.15; H, 5.14; N, 11.07. Found (%): C, 71.95; H, 5.32; N, 10.91.

Synthesis of metal complexes: The Schiff base metal complexes were prepared in accordance with the reference[20,21] methods. The 0.506 g (1 mmol) of Schiff base ligands were dissolved in 30 mL ethanol and then added drops into the solution with 0.249 g (1 mmol) $Co(OAc)_2{\cdot}4H_2O$ aqueous solution of 20 mL within 0.5 h. After the mixture solution was continue stirred at 60 °C for 6 h, then cooling and filtering. The solid product was washed with ethanol and distilled water several times and dried in a vacumm over at 60 °C, to get brown powder solids $CoL{\cdot}H_2O$. Yield: 0.452 g, yield: 77.5 %. The Schiff base manganese complexes ($MnL{\cdot}H_2O$) was prepared with the the same methods, to get 0.421 g dark green powder solid product in 72.5 % yield (**Scheme-I**).

Method of calculations: The molecular geometry for all complexes and ligand were fully optimized at 6-311+G (d, p) basis set using becke's three-parameter-hybird (B3LYP) of density functional theory (DFT) method[22,23]. Self consistent field convergence criteria for 10^{-8} and the frequency analysis to determine the stagnation point for stable configuration. Furthermore, the charge transfer interactions between the related orbitals, electron density and the essential of the correlative bond length changes in the complexes were detailed discussed using the natural bond orbital theory (NBO) and corresponding to software. The calculation result is not affected by the basis set and dispersion function, research results are reliable. All calculations were performed using Gaussian 03 software. The Gaussian 03W packsge was employed to perform optimization of structure and all the calculations[24]. The optimized structure of Schiff base ligand H_2L and relate to metal complex $CoL{\cdot}H_2O$ are shown in Fig. 2.

RESULTS AND DISCUSSION

^{1}H-NMR of the Schiff base H_2L ligand: The ^{1}H-NMR data of ligand (Fig. 1) recorded in DMSO-d_6, show a sharp in 10.1-10.2 ppm which may be assigned to the carboxyl group and indule ring (-N-H-, 2H) protons, respectively. There is an obvious singlet peak at 8.6 ppm, showed the azomethine group (-CH=N-, 2H) proton chemical shift. The proton of benzene ring was seen in the range of 8.1-8.26 ppm as two close singlet peak. In the 7.1-7.8 ppm have multiple continuous coupling singlet peak, explored for the chemical shift on the indole ring. From the above analysis data, the Schiff base ligand of H_2L was synthesized successfully.

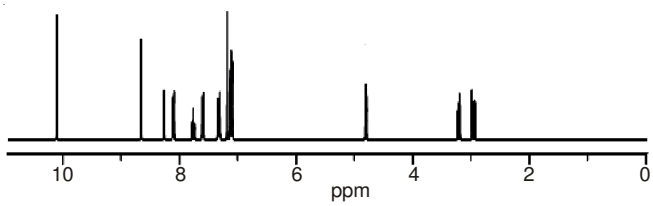

Fig. 1. ^{1}H-NMR spectral chart of H_2L ligand

IR spectra and mode of bonding analysis: The IR spectra of the studied compounds are listed in Table-1. IR spectra of complexes $CoL{\cdot}H_2O$ and $MnL{\cdot}H_2O$ showed a strong and wide absorption band at 3400 cm^{-1} that attributed to crystal water ν(H-O-H). It can be determined with crystal water in the complexes molecular of $CoL{\cdot}H_2O$ and $MnL{\cdot}H_2O$. The absence of band 3010 cm^{-1} for ligand H_2L due to ν(O-H) stretching vibration absorption, but in IR spectra of L-tryptophan showed a strong absorption band at 3079 cm^{-1}. In general, the ν(O-H) stretching vibration band range from 3200 to 2599 cm^{-1}. So there is carboxyl group (-COOH) in the H_2L ligand and the absorption band range shifted to lower wave numbers. However, the O-H bond of carboxyl group stretching vibration absorption bands has not showed in the corresponded metal complexes IR spectra. While the appearance of a medium band near 1387 cm^{-1} ($CoL{\cdot}H_2O$) and 1395 cm^{-1} ($MnL{\cdot}H_2O$) corresponding to ligand H_2L. It explained that carboxyl group in H_2L changed into carboxylate anion ($-COO^-$) for the ligand H_2L coordinated with Co(II) and Mn(II) cation. In addition, by comparing the asymmetric ν(C=O) stretching vibration absorption bands in Table-1, It was found that the absorption band of ligand H_2L had a lower frequency compared to those

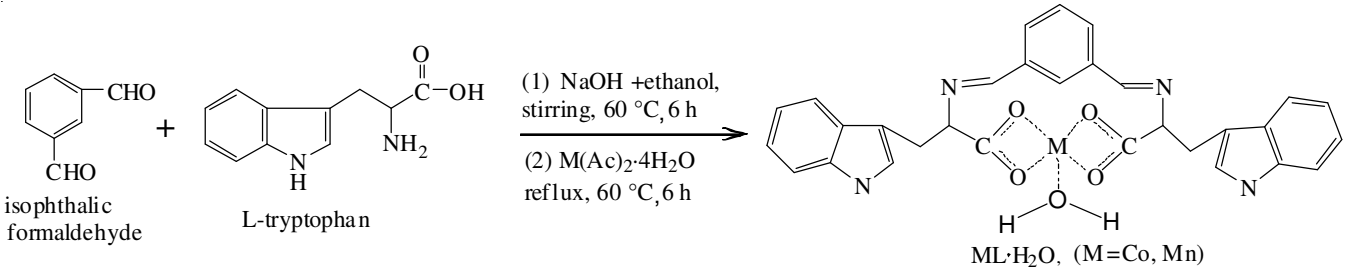

Scheme-I: Preparation route for complexes $CoL{\cdot}H_2O$ and $MnL{\cdot}H_2O$

of 1,3-benzenedialdehyde and L-tryptophan, mainly due to the formation of the intramolecular H-bonding between these two -COOH groups which caused the shift of ν(C=O) to lower wave numbers. Similarly, the asymmetric ν(C=O) stretching vibration bands of metal complexes $CoL·H_2O$ and $MnL·H_2O$ were found to be at 1610 and 1607 cm^{-1}, respectively, which was because that the two C-O bonds of the -COO- were identical while generally the absorption band fall within 1550-610 cm^{-1}. This phenomenon demonstrated that metal complexes were synthesized successfully.

Table-1 also showed that the ν(CH=N) stretching vibration absorption band of ligand H_2L was at 1601 cm^{-1} and the corresponding bands of the complex showed up at 1599 and 1598 cm^{-1}, which indicated that the absorption band of the complexes shifted to lower wave numbers. Furthermore, this result illustrated that the nitrogen atom of the ligand H_2L interacted with the metal ion to form M-N coordinate bond.

The bands ranged within 516-512 and 450-441 cm^{-1} in IR spectra of complexes $CoL·H_2O$ and $MnL·H_2O$ indicated the formation of new chemical bonds, which was attributed to their individual ν(M-O) and ν(M-N) absorption bands, respectively. Therefore, based on the above analysis of IR spectra data, we can see that ligand H_2L is a binegative hexadentate ligand with its active site at -OOOONN and coordinates with the metal ions through the interaction between O atom in -COO- group and N atom in CH=N group.

Thermal analysis (TG, DTG and DTA): Through the analysis of the Schiff base ligand H_2L and corresponding to complexes, we could obtain the thermal stability of these new complexes and the thermal decomposition of atoms or atomic chemical bonds and in the meanwhile, decide whether crystal water was present in the complexes. Additionally, previous studies showed that the metal complexes would lose weight when heated up to 80 °C due to the presence of crystal water[2]. The thermal properties of the Schiff base ligand and their complexes were investigated by thermograms (TG, DTG and DTA) and the corresponding thermal analysis data was presented in Table-2.

In the case of 1,3-benzenedialdehyde as shown in Table-2, the thermal gravimetric analysis showed only one decomposition stage which started at 80 °C and ended at 220 °C and the peak temperature was 210 °C, with the end products being CO_2 and NO.

The TG curve of the L-tryptophan showed three decomposition steps. The first step of decomposition within the temperature range 200-300 °C corresponded to the mass loss of L-tryptophan molecules by 28.9 % (calcd. 25.9 %) and the removal of amine group ($-NH_2$) and carboxyl group (-COOH) of the indole ring, with the end products being CO_2 and NH_3; while the second step of decomposition in the L-tryptophan occurred within the temperature range 300-450 °C with a further mass loss of 13.7 % (calcd. 14.3 %), which corresponded to the removal of ethyl group ($-CH_2-CH_3$) of the indole ring, with the end products being CO_2 and H_2O; the last step (450-900 °C) corresponded to the complete decomposition of the indole ring with the generation of CO_2 and NH_3 as gases and a mass loss of 57.4 % (calcd. 59.4 %).

The TG data of Schiff base ligand H_2L are listed in Table-2. The H_2L decomposes into three stages within the temperature range from 50 to 1000 °C. The first stage, at 100-475 °C with the peak temperature at 350 °C, corresponded to the loss of two carboxyl groups (-COOH) of ligand H_2L with a mass loss of 18.1 % (calcd. 18.6 %); while the subsequent stage within the temperature range 475-840 °C involves the

TABLE-1
IR DATA (4000-400 cm^{-1}) OF ISOPHTHALALDEHYDE, L-TRYPTOPHAN H_2L AND ITS METAL COMPLEXES

Compound	ν(H-O-H)	ν(O-H)	ν(CH=N)	νa_{svm}(C=O)	ν_{svm}(C=O)	ν(M-O)	ν(M-N)
Isophthalaldehyde	-	-	-	1694s	-	-	-
L-tryptophan	-	3079s	-	1692s	-	-	-
H_2L	-	3010 w	1598 m	1640s h	-	-	-
$CoL·H_2O$	3429 m	-	1599 m	1610s h	1387 m	512s h	450 w
$MnL·H_2O$	3434 m	-	1598 m	1607s h	1395 m	516s h	441 w

s: strong, m: medium, w: weak, sh: sharp

TABLE-2
THERMAL ANALYSIS DATA OF ISOPHTHALALDEHYDE, L-TRYPTOPHAN H_2L AND ITS METAL COMPLEXES

Compound	TG range (°C)	DTG_{max}	n	Mass loss (calcd. %)	Total mass loss (%)	Assignment	Metallic residue	DTA (°C)
1,3-Benzenedialdehyde L-tryptophan	80-220	210	1	100 (100)	100	Loss of $C_8H_6O_2$	-	90 (+), 190 (-)
	200-300	290	1	28.9 (25.9)	100	Loss of$C_2H_3O_2N$	-	289 (+), 450 (-)
	300-450	390	1	13.7 (14.3)		Loss of C_2H_5	-	550 (-)
	450-900	500	1	57.4 (59.5)		Loss of C_8H_7N	-	
H_2L	100-475	350	1	18.1 (18.6)	100	Loss of $C_2H_2O_4$	-	470 (+), 530 (-),
	475-840	530, 680	2	22.3 (21.9)		Loss of $C_6H_8N_2$	-	970 (-)
	840-1000	960	1	59.6 (59.5)		Loss of $C_{18}H_{16}N_2$	-	
$CoL·H_2O$	50-100	96	1	3.6 (3.2)	91.2	Loss of H_2O	CoO	270 (+), 400 (+),
	100-400	295	1	17.1 (15.4)	(87.0)	Loss of C_2O_4		500 (-), 960 (-)
	400-540	440	1	10.3 (9.5)		Loss of C_4H_6		
	540-1000	940	1	60.2 (63.2)		Loss fo $C_{24}H_{16}N_4$		
$MnL·H_2O$	50-100	97	1	4.1 (3.2)	89.6	Loss of H_2O	MnO	281 (+), 400 (+),
	100-500	340	1	12.5 (15.5)	(87.5)	Loss of C_2O_4		490 (-), 900 (-)
	500-1000	500, 900	2	73.0 (68.8)		Loss of $C_{28}H_{22}N_4$		

n = Number of decompositionsteps. (-) = exothermic peak, (+) = endothermic peak

loss of molecular fragment $C_6H_8N_2$ between the indole and benzene ring with an estimated mass loss of 22.3 % (calcd. 21.9 %) in two steps; the final stage, at 840-1000 °C, corresponded to the loss of fragment $C_{22}H_{16}N_2$ originating from the complete decomposition of indole and benzene ring, with the end products of decomposition being CO_2,H_2O and NO as gases and a mass loss of 59.6 % (calcd. 59.5 %). The DTA curve of the Schiff base ligand H_2L showed the endothermic peak displayed at 276 °C, while two exothermic peaks located at 530 and 970 °C, respectively.

The corresponding thermal gravimetric analysis data of complex CoL·H_2O were also presented in Table-2. Table-2 showed that the thermogram of CoL·H_2O showed four decomposition stages within the temperature range 50-1000 °C. The first stage of decomposition within the temperature range 50-100 °C corresponded to the removal of a molecule of water, with a mass loss of 3.6 % (calcd. 3.2 %). The second stage of decomposition within the temperature range 100-400 °C with a mass loss of 17.1 % (calcd. 15.4 %) had the highest decomposition temperature at 295 °C as shown in the DTA curve, which was attributed to the removal of carboxylate anion (-COO-) from the chelating Co(II) complexes. While the third stage within the temperature range 400-540 °C involved the loss of C_4H_6 with an estimated mass loss of 10.3 % (calcd. 9.5 %), which was attributed the loss of molecular fragment -CH_2-CH- between the ligand and indole ring; the last stage, at temperature 540-1000 °C, corresponded to the loss of fragment $C_{24}H_{16}N_4$ originating from the decomposition of indole and benzene ring, which was quite similar to the last stage of ligand H_2L decomposition, with a mass loss of 60.2 % (calcd. 63.2 %). The overall mass loss amounted to 82.90 % (calcd. 82.33 %) in terms of CoL·H_2O, while the remaining was the weight of CoO. Through the study of thermal analysis data, we could see that the uncoordinated ligand H_2L and Co(II) induced an increase of experimental amount compared with the theoretical amount. The DTA curve of the complexes CoL·H_2O showed two endothermic peaks displayed at 270 and 400 °C, respectively; while two exothermic peaks located at 500 and 960 °C, respectively.

Thermograms (TG, DTG and DTA) data of complexes MnL·H_2O were also shown in Table-2. The TG-DTA curves of MnL·H_2O represented three stages. The first step of decomposition within the temperature range 50-100 °C corresponded to the loss of crystal water with a mass loss of 4.1 % (calcd. 3.2 %), which further confirmed the presence of one crystal water molecule in MnL·H_2O. The second stage of decomposition was observed at 100-500 °C, with mainly the loss of CO_2 and a mass loss of 12.5 % (calcd. 15.5 %). While the mass losses of the remaining decomposition step amounted to 73 % (calcd. 68.8 %) and corresponded to the removal of $C_{28}H_{22}N_4$ molecules, which represented the complete decomposition of MnL·H_2O complexes within the temperature range 500-1000 °C. The overall mass loss amounted to 89.6 % (calcd. 87.5 %) with the remainder being MnO. As shown in the DTA curve of MnL·H_2O, two endothermic peaks were observed at 281 and 400 °C, respectively, meanwhile the other two strong exothermic peaks were observed at 490 and 900 °C, respectively. Clearly, the thermograms of MnL·H_2O complex was predominantly exothermic.

Theoretical results: The Schiff base ligand H_2L, Co(II) and Mn(II) complexes were chosen as the objects of study, as well as the spin multiplicity under the lowest energy state, so the spin multiplicity of Co(II) and Mn(II) complexes were 4 and 6, respectively. The total charge of these two complexes was zero, therefore, the calculated total energies (E) for CoL·H_2O and MnL·H_2O were found to be -3136.2 a.u and -2904.5 a.u., respectively.

Geometry optimization: Fig. 2 showed the front and side views of the geometries of the Schiff base ligand H_2L and its complex CoL·H_2O after optimization. Geometry data of MnL·H_2O complexes were not shown in Fig. 2 due to the structural similarities between CoL·H_2O and MnL·H_2O, while Fig. 1 presented some parameters of the optimized structure of ligand H_2L and CoL·H_2O complex. As shown in the optimized geometries in Fig. 2, OOOONN six-atom active sites in ligand H_2L were surrounded by one benzene and two indole rings, while the geometry structure was changed in the model after ligand H_2L coordinated with CoL·H_2O caused by Co(II) ions and H_2O molecules. Thus, Co(II) ions were located in the three-dimensional tetrahedral and coordinated with four oxygen atoms [Fig. 2(c) and (d)]. Table-3 indicated that the four O-Co(II) bonds, O38-Co63,O62-Co63,O61-Co63,O64-Co63, showed different bond lengths, that is 0.1931, 0.2064, 0.2075 and 0.1957 nm, respectively. It indicated that those four bonds were in different bond lengths. In addition to that, the angles of four bonds O61-Co63-O62, O62-Co63-O38, O38-Co63-O64 and O64-Co63-O61 were found to be 64.8º, 116.1º, 89.5º, 131.6º, respectively, which further indicated

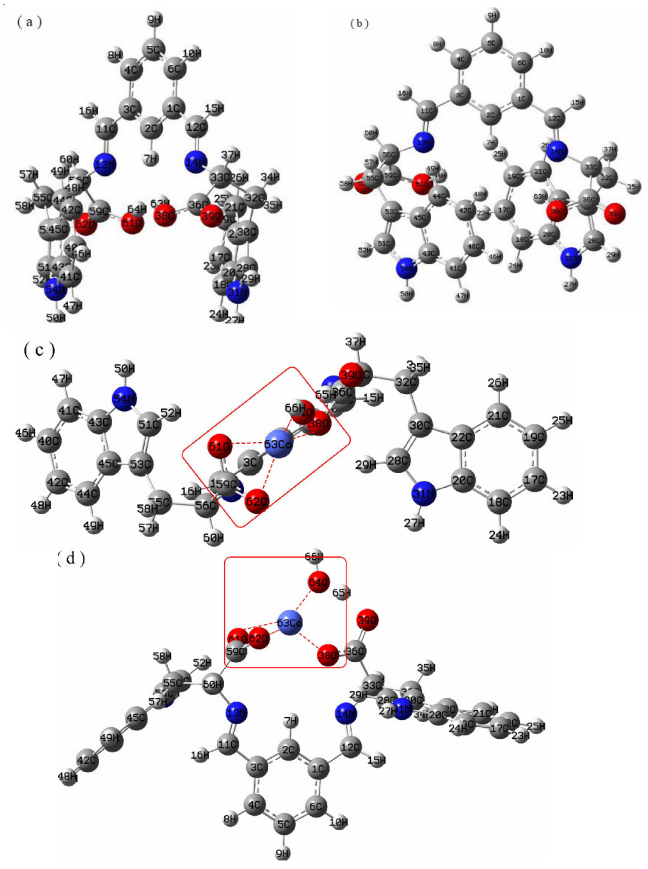

Fig. 2. The optimized structure of (a) H_2L side view; (b) H_2L front view; (c) CoL·H_2O top view and (d) CoL·H_2O fron view

TABLE-3
OPTIMIZED GEOMETRICAL PARAMETERS OF H_2L AND ITS METAL COMPLEXES

Compound	Bond length	Value(nm)	Bond angle	Value (º)	Dihedral angle	Value (º)
H_2L	C36-O38	0.1341	C12-N14-C33	118.2	C6-C1-C12-N14	174.8
	C36-O39	0.1211	C33-C36-O38	115.9	C1-C12-N14-C33	178.7
	C33-C36	0.1537	C33-C36-O39	121.9	N14-C33-C36-O38	12.4
	C12-N14	0.1277	O38-C36-O39	122.0	C33-C36-O38-O39	179.1
$CoL·H_2O$	C36-O38	0.1305	C33-C36-O39	119.3	C1-C12-N14-C33	167.3
	C36-O39	0.1279	O38-C33-O39	122.7	N14-C33-C36-O38	21.2
	O38-Co63	0.1931	C56-C59-O61	122.5	O38-O39-O61-O62	54.2
	O39-Co63	0.3321	C56-C59-O62	120.3	O38-C36-O39-Co63	10.1
	C59-O62	0.1303	O61-C59-O62	116.4	N13-C11-N14-C12	40.5
	C59-O61	0.1305	O61-Co63-O62	64.8	O38-O39-O64-Co63	6.5
	O62-Co63	0.2064	O62-Co63-O38	116.1	O61-O62-Co63-O64	125.8
	O61-Co63	0.2075	O38-Co63-O64	89.5	O61-O62-O38-O64	80.3
	O64-Co63	0.1957	O64-Co63-O61	131.6	O61-O62-O38-O39	89.1
$MnL·H_2O$	C36-O38	0.1303	C33-C36-O39	119.1	C1-C12-N14-C33	170.1
	C36-O39	0.1281	O38-C33-O39	122.4	N14-C33-C36-O38	25.9
	O38-Mn63	0.1998	C56-C59-O61	122.3	O38-O39-O61-O62	46.8
	O39-Mn63	0.3377	C56-C59-O62	119.4	O38-C36-O39-Mn63	13.2
	C59-O62	0.1305	O61-C59-O62	117.4	N13-C11-N14-C12	37.6
	C59-O61	0.1300	O61-Mn63-O62	62.3	O38-O39-O64-Mn63	8.4
	O62-Mn63	0.2133	O62-Mn63-O38	117.2	O61-O62-Mn63-O64	117.1
	O61-Mn63	0.2187	O38-Mn63-O64	87.6	O61-O62-O38-O64	77.0
	O64-n63	0.2048	O64-Mn63-O61	127.4	O61-O62-O38-O39	76.8

Co(II) was located in a distorted three-dimensional tetrahedral field. In terms of dihedral angle, both benzene and indole ring remained unchanged, while the coordinated atoms changed dramatically. On one hand, H_2L belonged to C2 point group; on the other hand, $CoL·H_2O$ belonged to C1 point group with dihedral angles of O61-O62-O38-O64 (64.8º) and O61-O62-Co63-O64 (125.8º), respectively; thus, the four oxygen atoms coordinated with Co(II) ions were located at the four vertices of the tetrahedron.

Electronic properties and Mulliken atomic charges for the complexes: Results from previous studies showed that, both HOMO (the highest occupied molecular orbital) and LUMO (the lowest-lying unoccupied molecular orbital) on the frontier molecular orbitals were very important parameters that were generally associated with the chemical reactivity and kinetic stability of a molecule. HOMO energy represents the ability to donate an electron which was associated with the ionization potential of molecules, while the energy of LUMO represented the ability to accept an electron that was directly related to the electron affinity. In addition, the energy difference between HOMO and LUMO orbitals, the energy gap, helps us to characterize the stability of molecular structures. The corresponding calculation method for energy gap is HOMO energy minus LUMO energy[25-29].

In order to obtain the stability and chemical reactivity of complexes $CoL·H_2O$ and $MnL·H_2O$, the frontier molecular orbital energies of them were calculated, respectively. The HOMO (EHOMO) and LUMO (ELUMO) energies of $CoL·H_2O$ were found to be -0.193 and -0.068 a.u, respectively; while those of MnLoH2O were found to be -0.192 and -0.047 a.u, respectively. According to the data shown above, the energy gap between HOMO and LUMO for the two complexes was actually very small, which indicated that both of the complexes were of low kinetic stability, high chemical reactivity and polarizability[27]. Thus, it would be a great benefit to the development of new catalysts. Additionally, to better understand the reactivity atoms of the metal complexes, the frontier molecular orbital energy diagram and energy gap were shown in Fig. 3. The highest occupied molecular orbital (HOMO) was mainly occupied by electrons from the indole ring, while the lowest unoccupied molecular orbital (LUMO) was occupied by the empty orbitals of Co(II) ions. Electron transfer from HOMO to LUMO suggested a process that electrons were transferred from the indole ring to the unoccupied orbitals of Co(II) with an energy gap of 0.125 a.u, resulting in a high chemical reactivity and polarizability of $CoL·H_2O$ complex.

As shown in Fig. 4, the Mulliken charge distribution of $CoL·H_2O$ complex was conducted in order to calculate the charge distribution of all atoms that could better help us understand the electron transfer process between the coordinating atoms and central Co(II) atoms[30-31]. Fig. 3 showed that the

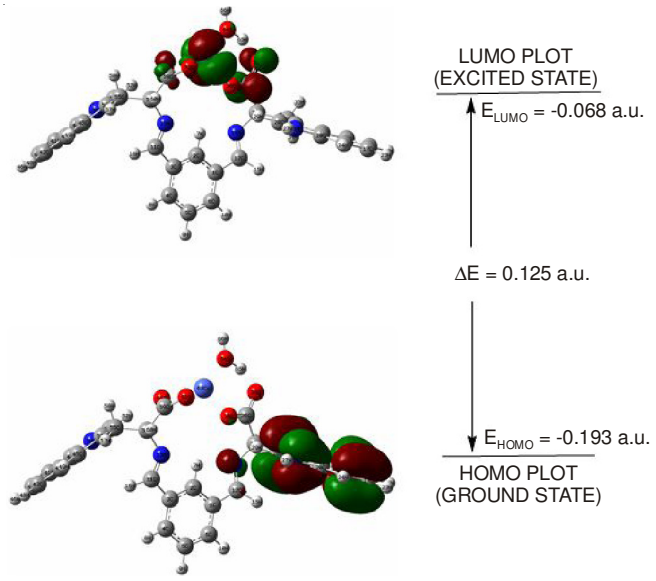

Fig. 3. Atomic orbital compositions of the frontier molecular orbital of $CoL·H_2O$

TABLE-4
WIBERG BOND INDEX FOR CoL·H_2O AND MnL·H_2O AT B3LYP/6-31+G(d, p) LEVEL

Compound	Wiberg						
	O38-M	O39-M	O61-M	O62-M	O64-M	N13-M	N14-M
CoL·H_2O	0.3170	0.0102	0.2588	0.2765	0.2884	0.0049	0.0018
MnL·H_2O	0.2492	0.0109	0.1952	0.2370	0.2256	0.0061	0.0031

M=Co, Mn

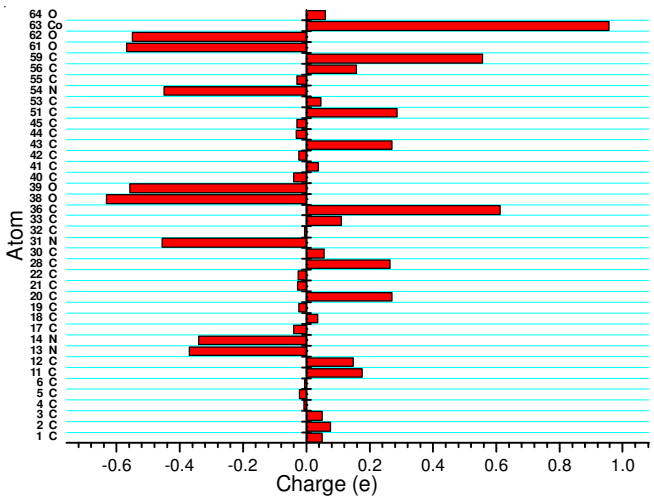

Fig. 4. Mulliken atomic charge distribution of CoL·H_2O

charge numbers of Co60, O38, O61, O62 and O64 were found to be 0.9569e, -0.6315e, -0.5684e, -0.5487e and -0.8234e, respectively. Based on the above data we could see that, the central metal ions lost 1.0431e (2.0000-0.9569) in terms of positive charge number, while the four coordinating oxygen atoms relatively went through a decrease of negative charge number with the largest negative charge number decrease seen in O62. Therefore, the Mulliken charge distribution illustrates that Co(II) coordinates to four of the oxygen atoms.

NBO analysis: Natural bond orbital (NBO) analysis was employed to study the bond formation mechanism and the distribution of electron density in atoms and in bonds between atoms, as well as the change of bond length and angle. Wiberg bond orders for metal complexes were calculated and presented in Table-4. Wiberg bond for the O-Co bond of CoL·H_2O complex was found to be within the range 0.3170-0.0102 as shown in Table-4, which was lower than the standard bond order (1.0) while close to the order of coordination bond[32]. Thus, the presence of the coordination bond between oxygen and Co atom, as well as the significant role of the four oxygen atoms (O38, O61,O62,O64) in coordinating with the Co atom as electron donors, was well explained. Due to the distance between N13, N14 atoms and Co(II) ion, Wiberg bond for the N-Co bond was relatively weak but not negligible. In addition, the property of MnL·H_2O complex is similar to that of CoL·H_2O as described above and thus not given unnecessary details.

Conclusion

The two new metal complexes of novel Schiff base with Co(II) and Mn(II) were prepared and formulated as CoL·H_2O and MnL·H_2O. The complexes have been characterized using elemental analysis, IR, ^{1}H NMR, thermal analyses. To study the structural and electronic properties of studied molecules, complete analysis of the TG-DTA/DTA, mulliken atomoc charges, Wiberg bond, NBO and HOMO-LUMO energy gap of CoL·H_2O and MnL·H_2O compounds. All theoretical calculations were carried out by the popular DFT methods, B3LYP at 6-311 level of theory. The applied method is in good accordance with experimental values. The HOMO-LUMO energy gap showed that the indole ring to the unoccupied orbitals of Co(II) with an energy gap of 0.125 a.u, resulting in a high chemical reactivity and polarizability of CoL·H_2O complex. The Mulliken charge illustrates that Co(II) coordinates to four oxygen atoms of H_2L, the four oxygen atoms coordinated with Co(II) ions were located at the four vertices of the tetrahedron.

ACKNOWLEDGEMENTS

The authors thank the National Nature Science Foundation of China (51063006) and the key Subject Foundation of Tianshui Normal University (TSA0818) for providing financial support for this project.

REFERENCES

1. B. Zhang, S. Li, E. Herdtweck and F.E. Kühn, *J. Organomet. Chem.*, **739**, 63 (2013).
2. A.H. Kianfar, S. Ramazani, R.H. Fath and M. Roushani, *Spectrochim. Acta A*, **105**, 374 (2013).
3. G. Romanowski and J. Kira, *Polyhedron*, **53**, 172 (2013).
4. W.L. Man, W.W.Y. Lam and T.C. Lau, Acc. Chem. Res., (In press) (2013).
5. R.K. Dubey, A.P. Singh and S.A. Patil, *Inorg. Chim. Acta*, **410**, 39 (2014).
6. V.P. Singh, S. Singh, D.P. Singh, K. Tiwari and M. Mishra, *J. Mol. Struct.*, **1058**, 71 (2014).
7. H.P. Ebrahimi, J.S. Hadi, Z.A. Abdulnabi and Z. Bolandnazar, *Spectrochim. Acta A*, **117**, 485 (2014).
8. S. Thalamuthu, B. Annaraj and M.A. Neelakantan, *Spectrochim. Acta A*, **118**, 120 (2014).
9. R.M. Wang, X.D. Li and Y.F. He, *Chin. Chem. Lett.*, **17**, 265 (2006).
10. L. Lekha, K. Kanmani Raja, G. Rajagopal and D. Easwaramoorthy, *J. Organomet. Chem.*, **75**, 72 (2014).
11. H. Naeimi and A. Karshenas, *Polyhedron*, **49**, 234 (2013).
12. G.Q. Jiang, S.J. Li, Y.Q. Zhang and Q.J. Zhang, *Inorg. Chem. Commun.*, **40**, 172 (2014).
13. O.V. Levin, M.P. Karushev, A.M. Timonov, E.V. Alekseeva, S.H. Zhang and V.V. Malev, *Electrochim. Acta*, **109**, 153 (2013).
14. X.D. Cai, H.Y. Wang, Q.P. Zhang, J.H. Tong and Z.Q. Lei, *J. Mol. Catal. Chem.*, **383-384**, 217 (2014).
15. A. Ourari, M. Khelafi, D. Aggoun, A. Jutand and C. Amatore, *Electrochim. Acta*, **75**, 366 (2012).
16. Y. Chang, Y.R. Lv, F. Lu, F. Zha and Z.Q. Lei, *J. Mol. Catal. Chem.*, **320**, 56 (2010).
17. M. Salavati-Niasari, E. Esmaeili, H. Seyghalkar and M. Bazarganipour, *Inorg. Chim. Acta*, **375**, 11 (2011).
18. S.E. Schaus, B.D. Brandes, J.F. Larrow, M. Tokunaga, K.B. Hansen, A.E. Gould, M.E. Furrow and E.N. Jacobsen, *J. Am. Chem. Soc.*, **124**, 1307 (2002).
19. T. Katsuki, *J. Mol. Catal. Chem.*, **113**, 87 (1996).
20. D. Wöhrel, H. Bohlen, C. Aeinger and D. Pohl, *Makromol. Chem.*, **185**, 699 (1984).
21. Y. Maeda, M. Miyamoto, Y. Takashima and H. Oshio, *Inorg. Chim. Acta*, **204**, 231 (1993).

22. T. Schaefer, S.R. Salman, T.A. Wildman and P.D. Clark, *Can. J. Chem*., **60**, 342 (1982).
23. J.D. David and H.E. Hallam, *Spectrochim. Acta A*, **21**, 841 (1965).
24. M.J. Frisch, G.W. Trucks, H.B. Schlegel, G.E. Scuseria, M.A. Robb, J.R. Cheeseman, J.A. Montgomery Jr., T. Vreven, K.N. Kudin, J.C. Burant, J.M. Millam, S.S. Iyengar, J. Tomasi, V. Barone, B. Mennucci, M. Cossi, G. Scalmani, N. Rega, G.A. Petersson, H. Nakatsuji, M. Hada, M. Ehara, K. Toyota, R. Fukuda, J. Hasegawa, M. Ishida, T. Nakajima, Y. Honda, O. Kitao, H. Nakai, M. Klene, X. Li, J.E. Knox, H.P. Hratchian, J.B. Cross, V. Bakken, C. Adamo, J. Jaramillo, R. Gomperts, R.E. Stratmann, O. Yazyev, A.J. Austin, R. Cammi, C. Pomelli, J.W. Ochterski, P.Y. Ayala, K. Morokuma, G.A. Voth, P. Salvador, J.J. Dannenberg, V.G. Zakrzewski, S. Dapprich, A.D. Daniels, M.C. Strain, O. Farkas, D.K. Malick, A.D. Rabuck, K. Raghavachari, J.B. Foresman, J.V. Ortiz, Q. Cui, A.G. Baboul, S. Clifford, J. Cioslowski, B.B. Stefanov, G. Liu, A. Liashenko, P. Piskorz, I. Komaromi, R.L. Martin, D.J. Fox, T. Keith, M.A. Al-Laham, C.Y. Peng, A. Nanayakkara, M. Challacombe, P.M.W. Gill, B. Johnson, W. Chen, M.W. Wong, C. Gonzalez and J. A. Pople, Gaussian 03, E.01, Gaussian, Inc., Wallingford CT (2004).
25. M. Govindarajan and M. Karabacak, *Spectrochim. Acta A*, **96**, 421 (2012).
26. M. Govindarajan, S. Periandy and K. Carthigayen, *Spectrochim. Acta A*, **97**, 411 (2012).
27. I. Fleming, Frontier Orbitals and Organic Chemical Reactions, John Wiley & Sons, New York (1976).
28. L.A. Curtiss, P.C. Redfern, K. Raghavachari and J.A. Pople, *J. Chem. Phys.*, **109**, 42 (1998).
29. C. Ravikumar, I.H. Joe and V.S. Jayakumar, *Chem. Phys. Lett*., **460**, 552 (2008).
30. R.S. Mulliken, *J. Chem. Phys.*, **23**, 1833 (1955).
31. A. Lakshmi and V. Balachandran, *J. Mol. Struct*., **1033**, 40 (2013).
32. K.B. Wiberg, *Tetrahedron*, **24**, 1083 (1968).